Nanoscale

RSC Publishing

PAPER

View Article Online
View Journal | View Issue

Cite this: *Nanoscale*, 2013, **5**, 3976

Electroactive nanoparticle directed assembly of functionalized graphene nanosheets into hierarchical structures with hybrid compositions for flexible supercapacitors†

Bong Gill Choi,[a] Yun Suk Huh,[b] Won Hi Hong,[a] David Erickson*[c] and Ho Seok Park*[d]

Hierarchical structures of hybrid materials with the controlled compositions have been shown to offer a breakthrough for energy storage and conversion. Here, we report the integrative assembly of chemically modified graphene (CMG) building blocks into hierarchical complex structures with the hybrid composition for high performance flexible pseudocapacitors. The formation mechanism of hierarchical CMG/Nafion/RuO_2 (CMGNR) microspheres, which is triggered by the cooperative interplay during the *in situ* synthesis of RuO_2 nanoparticles (NPs), was extensively investigated. In particular, the hierarchical CMGNR microspheres consisting of the aggregates of CMG/Nafion (CMGN) nanosheets and RuO_2 NPs provided large surface area and facile ion accessibility to storage sites, while the interconnected nanosheets offered continuous electron pathways and mechanical integrity. The synergistic effect of CMGNR hybrids on the supercapacitor (SC) performance was derived from the hybrid composition of pseudocapacitive RuO_2 NPs with the conductive CMGNs as well as from structural features. Consequently, the CMGNR-SCs showed a specific capacitance as high as 160 F g^{-1}, three-fold higher than that of conventional graphene SCs, and a capacitance retention of >95% of the maximum value even after severe bending and 1000 charge–discharge tests due to the structural and compositional features.

Received 16th November 2012
Accepted 22nd February 2013

DOI: 10.1039/c3nr33674c

www.rsc.org/nanoscale

Introduction

Hierarchical, complex structures of hybrid materials with the controlled chemical compositions have been shown to offer a breakthrough for energy storage and conversion.[1–4] Such a structural hierarchy is extremely crucial for achieving the significant features of electrodes such as large surface area, easy accessibility to reaction sites, facilitated mass and ion transport, and mechanical integrity.[1] In contrast, appropriate hybrid compositions lead to the synergistic performance of constitutive multicomponents by means of controlling interfacial interactions.[5–7] In particular, the combination of conflicting, but essential characteristics such as electronic and ionic, energetic and powerful, or double layer capacitive and pseudocapacitive properties has been regarded as a novel approach for resolving the current challenges by the hybrid composition.[8] Accordingly, the controlled assembly of electrical double layer capacitive nanomaterials driven by electroactive nanoparticles (NPs) is expected to deliver high performance electrode materials in terms of harmonizing the structure of nanoscale building blocks with the chemical composition of the resulting hybrids.[9–11]

In this paper, it is postulated that the electroactive NP-directed assembly of graphene building blocks into hierarchical structures enables us to resolve a big hurdle for the realization of high performance flexible supercapacitors (SCs). Despite the higher power, faster rate capability, and better cycle stability of SCs than those of lithium rechargeable batteries, the practical application of SCs is exceedingly limited by low energy density.[12,13] In order to improve the capacitance for high energy density, the electroactive (or pseudocapacitive) materials such as metal oxides and conducting polymers, which can store energy through a faradaic reaction on the surface, have been hybridized with the highly conductive and electrical double layer capacitive materials.[14,15] Another important issue is the development of flexible energy storage devices for emerging applications into flexible mobile and portable systems.[16–22] Besides the aforementioned drawbacks of SCs, the realization of flexible devices still remains a critical challenge due to the low

[a]*Department of Chem. & Biomolecular Eng. (BK 21), Korea Advanced Institute of Science and Technology, Daejeon 305-701, Republic of Korea*

[b]*Department of Biological Engineering, College of Engineering, Inha University, Incheon, Republic of Korea*

[c]*School of Mechanical and Aerospace Engineering, Cornell University, Ithaca, NY 14853, USA. E-mail: de54@cornell.edu*

[d]*Department of Chemical Engineering, College of Engineering, Kyung Hee University, Yongin-si 446-701, Republic of Korea. E-mail: phs0727@khu.ac.kr*

† Electronic supplementary information (ESI) available: Electrodeposition procedure, TEM, SEM, and AFM images, XPS, FT-IR, and XRD spectra, mechanical strain–stress curve, textural and conductive properties, and impedance spectroscopy. See DOI: 10.1039/c3nr33674c

processability and intrinsic inflexibility of electrodes.[16–18] Although we and other groups demonstrated the fabrication of flexible SCs using graphene electrodes, the capacitances should be enhanced further as previous results were obtained from electrical double layer SCs, not from pseudocapacitors.

Herein, we report a straightforward and useful method for the electroactive NP-directed assembly of graphene nanosheets in a hierarchically structured manner, concomitantly with the well-defined chemical compositions. Two key aspects of this method for flexible energy storage devices are considered here: hierarchical structures offer large surface area and easy accessibility of ions to storage sites, while the hybrid compositions of conductive graphenes and electroactive NPs provide high capacitance, stable cycling performance, and flexibility. Chemically modified graphenes (CMGs) were used as conductive, nanoscale building blocks, whose structures were simply tuned by electroactive RuO_2 NPs. In particular, RuO_2 acted as structure guiding materials for hierarchical morphology as well as electroactive NPs for pseudocapacitance. The application of CMG/RuO_2 hybrids in SC electrodes was previously demonstrated by us and other groups,[23–25] but the assembly into hierarchical structures and the configuration of solid-state flexible devices have been unexplored yet.

Experimental section

Synthesis of hierarchically structured CMG/Nafion/RuO_2 (CMGNR) hybrids

Briefly, single layers of graphene oxides (GOs) were obtained from the commercial graphite powder, following the modified Hummers method as previously described in our reports.[26–28] The as-prepared GOs of 10 mg were dispersed in 20 mL of deionized (DI) water and 1-propanol (volume ratio of 50 : 50). 30 wt% of Nafion was mixed with 0.5 mg mL^{-1} of GOs in bisolvents. The homogeneous solution of GO and Nafion was prepared by sonication for 60 min and subsequently chemically reducing the mixture by addition of 100 μL of hydrazine solution at 85 °C for 24 h. The resulting mixture was washed with DI water and ethanol several times, and purified by dialysis for one week. 2 mg of CMG/Nafion (CMGN) hybrids was suspended in 2 mL of DI water and 2 mL of 1-propanol. The solution was mixed with 5×10^{-3} mmol of $RuCl_3 \cdot xH_2O$ solution. The resulting mixtures were sonicated for 10 min (Fisher Scientific Model 500 ultrasonic). The as-obtained hybrids were repeatedly washed with DI water and then filtered. The CMGNR hybrids were obtained after annealing in air at 300 °C for 2 h.

Fabrication of CMGNR-SC devices

CMGNR films were prepared by filtering homogeneous solutions in DI water–1-propanol (volume ratio of 50 : 50) bisolvents through an anodisc membrane filter (47 mm in diameter, 0.2 μm pore size, Whatman). The as-obtained thin films were placed directly into a bath of 3 M NaOH. The NaOH solution was exchanged with DI water by recirculation until the pH was near 7.0. A piece of a poly(ethylene terephthalate) (PET) substrate was immersed into the water and allowed to sink to the bottom of the bath. The CMGNR film deposited on PET was obtained after the DI water was drained. The thin gold films were deposited on the edge of each CMGNR films transferred into PET substrates for electrical contact through the electron-beam evaporation technique. The resulting thin films were dried in a vacuum at 60 °C and then directly used as electrode materials without any binders and additional carbons. The CMGNR-SCs were fabricated by integration of the Nafion 115 membrane (E. I. Dupont de Nemours and Co.) with two CMGNR films through a hot-pressing method. The detailed information is described below. Prior to the use of the Nafion 115 membrane, the membrane was boiled in 30% H_2O_2 for about 1 h at about 70–80 °C and then immersed in 1 M H_2SO_4 solutions for 1 h. Then they were cleaned for 1 h in high purity DI water between each step. The solid Nafion electrolyte membrane was sandwiched with the two CMGNR films and then integrated through a hot pressing procedure at 100 kg cm^{-2} and 130 °C for 3 min, which results in the close contact between the electrolyte and electrode for the film consolidation. The resulting solid-state flexible CMGNR-SCs consist of CMGNR as an electrode and the Nafion membrane as both an electrolyte and a separator. CMG-SCs, CMGN-SCs, and CMGN/RuO_2-SCs used as control samples were prepared following the same protocols as CMGNR-SCs. The weight of RuO_2 for CMGN/RuO_2 was accurately determined (Sartorius Genius, ME235S) in order to compare with CMGNR.

Characterization

TEM images were collected on an E.M. 912 Ω energy-filtering TEM (EF TEM 120 kV). SEM images were obtained using a field emission scanning electron microscope (FEI Sirion model) equipped with an in-house Schottky emitter in high stability. The X-ray diffraction (XRD) data were obtained on a Rigaku D/max lllC (3 kW) with a θ/θ goniometer equipped with a CuKα radiation generator. The diffraction angle of the diffractograms was in the range of $2\theta = 5°$ to 40°. The X-ray photoelectron spectroscopy (XPS) data were obtained using a Thermo Multi-Lab 2000 system. An Al Mgα X-ray source at 200 W was used with a pass energy of 20 eV and a 45° takeoff angle under 10^{-7} Torr vacuum analysis chamber. Thermogravimetric analysis (TGA) was carried out using a Dupont 2200 thermal analysis station. N_2 adsorption/desorption was determined by Brunauer–Emmett–Teller (BET) measurements using an ASAP-2010 surface area analyzer. The BET method was used to calculate the specific surface area of samples. The pore size distributions were induced by the Barrett–Joyner–Halenda (BJH) model. Electrical conductivities of the films were measured by the standard four-point probe technique (Loresta-GP, Mitsubishi Chemical). The electrochemical characteristics of SC devices under a two-electrode system using wetted Nafion membranes were evaluated by CV using a CHI 760D electrochemical workstation (CH Instruments) and galvanostatic charge–discharge using a Solartron 1260 at RT.

Results and discussion

The procedures for controlling the structures of CMG building blocks during the fabrication of flexible conductive films are

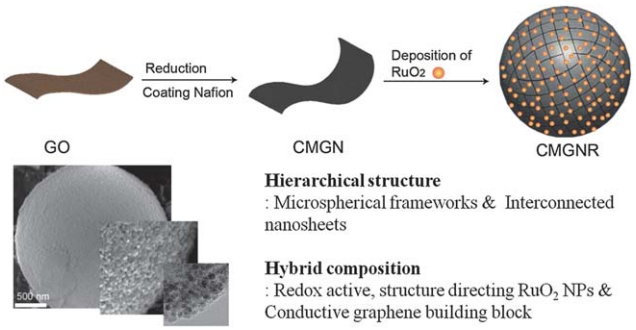

Fig. 1 Schematic procedures for illustrating the synthesis of hierarchical CMGNR microspheres through supramolecular assembly.

illustrated in Fig. 1. We demonstrated the fabrication of CMGN hybrid films and the favorable interactions between CMG and Nafion as previously reported.[26,27] The composition of Nafion in CMGN hybrids was chosen to be 15 wt%, as the assembly of CMGNR hybrids into hierarchical structures was promoted by the interaction between CMGNs (not CMG) and RuO_2 NPs and with different scales without further morphological evolution, whereas no morphological transformation was observed without the synthesis of RuO_2 NPs. The as-synthesized microspherical CMGNR hybrid films were fabricated as pseudocapacitive electrodes. Consequently, the microspherical structure of CMGNR hybrids was triggered by the cooperative interplay during the *in situ* synthesis of RuO_2 NPs.

The hierarchical structures of CMGNR microspheres were extensively characterized by electron microscopic methods. By the addition of RuO_2 NPs of ~25 wt% (ESI, Fig. S1†), the CMGN nanosheets were aggregated with RuO_2 NPs and organized into microspheres to minimize the free energy as shown in Fig. 2. The coexistence of microspheres and sheet-like aggregates provided clear evidence of RuO_2 NP-directed assembly into hierarchical structures (Fig. 2a). As shown in the enlarged SEM images of CMGNR microspheres, the constituent CMGN nanosheets were obviously visible and randomly oriented, resulting in the rough surface of microspheres (Fig. 2b and c). As shown in the XRD pattern (Fig. 2d), the nanocrystalline structure of RuO_2 NPs was assigned to the rutile-type RuO_2 (JCPDS no. 40-1290).[29] As shown in the TEM image in Fig. 3, CMGNR microspheres were not hollow, but filled with the self-organized nanosheets. A high resolution (HR) TEM image showed that RuO_2 NPs of ~2 nm were aggregated and reorganized with CMGN nanosheets (Fig. 3b). For the minimization of surface energy, the aggregates of CMGN nanosheets and RuO_2 NPs were co-assembled into the microspherical structure in a hierarchical manner. The RuO_2 NP-directed assembly into the hierarchical spheres led to a nanoporous structure, showing dramatic increases in the surface area and pore volume from 9.56 $m^2\ g^{-1}$ and 0.04 $cm^3\ g^{-1}$ of CMGN films to 494.05 $m^2\ g^{-1}$ and 0.49 $cm^3\ g^{-1}$ of CMGNR films (ESI, Table S1†). The high mesoporosity of CMGNR films was attributed to the intersheet voids confined in microspheres (ESI, Fig. S2†, N_2 sorption–desorption), while the macroporosity was derived from intersphere voids. Additionally, the electrical conductivity of CMGNR films was evaluated to be 798 S m^{-1}, which is lower than that of CMGN films (1020 S m^{-1}) because of the incorporation of RuO_2 NPs with low electrical conductivity. However, it is worthwhile noting that the macropores of hierarchical CMGNR microspheres can provide the facile accessibility of ions to the adsorption sites, while their nanopores can offer a large surface area for charge storage.

In order to further investigate the structural formation in a hierarchical manner, scanning TEM (STEM) and XPS data spectra were observed. In this research, RuO_2 NPs of >25 wt% directed the reorganization of CMGN nanosheets into the microspherical structure through specific interactions. The complementary interplay of CMGNR hybrids was induced by the hydrogen bonding interactions between sulfonic groups of Nafion coated on CMG nanosheets and oxide groups of RuO_2

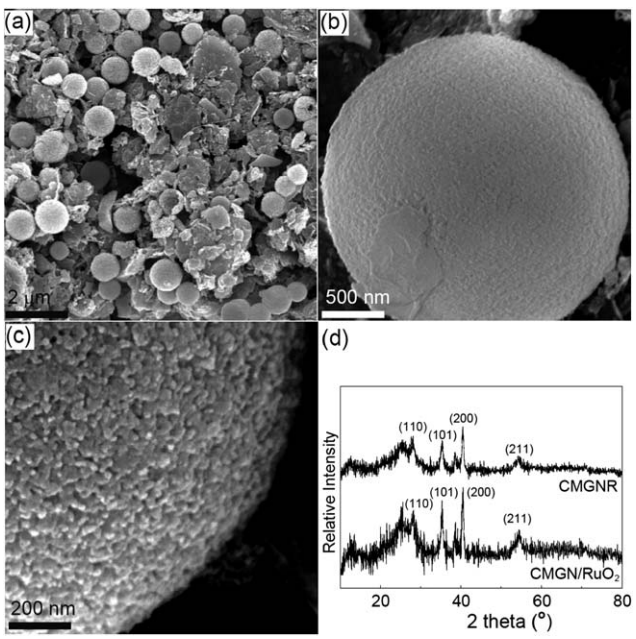

Fig. 2 (a) Surface SEM image of the CMGNR film. (b and c) High-magnification SEM images of individual CMGNR hybrids with a 3D hierarchical structure. (d) XRD pattern of CMGNR and CMGN/RuO_2 hybrids.

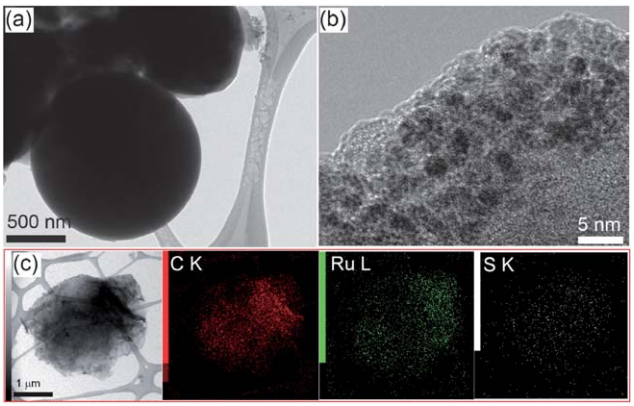

Fig. 3 (a and b) TEM images of CMGNR microspheres. (c) STEM image with EDS mapping (C, Ru, and S) for CMGNR hybrid sheets.

NPs, as confirmed by XPS spectra (ESI, Fig. S3†). It can be also supported by the C, S, and Ru mapping of the STEM image, where RuO_2 nanocrystals were uniformly distributed over the hybrid layers and the location of the Ru element was in good agreement with those of S and C elements (Fig. 3c). RuO_2NPs were strongly deposited on the surface of CMGN nanosheets. Moreover, no structural transformation into a spherical morphology was observed in the absence of Nafion. These results indicate that the specific interactions between CMGN nanosheets and RuO_2 NPs were critical for inducing the controlled assembly of 2D building blocks.

Another significant feature of CMGNR microspheres is the composition control of each constituent, because it strongly influences the formation of hierarchical spheres by means of the secondary force balance between CMGNs and RuO_2 NPs as well as the electrochemical performance of CMGNR microspheres as a consequence of the combination of pseudocapacitive RuO_2 NPs with the conductive CMGNs. Considering the electrical conductivity and structural formation, 15 wt% of Nafion became the optimal composition. Although the hierarchical structure was successfully constructed in the composition range of 25–35 wt% of RuO_2 NPs through the favorable interactions with CMGN building blocks, the surface area of CMGNR microspheres decreased above 25 wt% of RuO_2 NPs because of the pore filling or blockage by excess RuO_2 NPs. Consequently, the hybrid composition of CMGNR microspheres was controlled here into 15 wt% of Nafion, 60 wt% of CMG, and 25 wt% of RuO_2 NPs to accomplish the hierarchical structure and good physical properties.

Taking the full advantages of CMGNR microspheres, we fabricated pseudocapacitor devices integrated by flexible CMGNR thin films as electrodes and Nafion membrane as solid electrolytes (Fig. 4a). Details of the fabrication of flexible SCs are provided in the ESI.† The CMG-SCs and CMGN–SCs as control samples were tested under identical conditions. The specific capacitance (C_S) of the one electrode cell was calculated by using the following equation:[14]

$$C_S = I/[m(\Delta V/\Delta t)]$$

where I, m, and $\Delta V/\Delta t$ are the applied current density, the weight of electrode, and the discharge slope after IR drop, respectively. The CMGN–SCs exhibited a higher specific capacitance of 86.8 F g^{-1} compared to 56.4 F g^{-1} of CMG-SCs at 1 A g^{-1} (Fig. 4c and d). In this work, the specific capacitance of CMGN–SCs was lower than that of our previous work due to different chemical compositions.[17] Remarkably the CMGNR-SCs had a higher specific capacitance of 160 F g^{-1}, approximately two- and three-fold higher than those of CMGN–SCs and CMG-SCs, because of the large surface area of hierarchical spheres and pseudocapacitance of RuO_2 NPs (Fig. 4e). In the case of CV, the capacitance performance of CMGNR-SCs was also higher than those of CMG-SCs and CMGN–SCs (ESI, Fig. S4 and S5†), displaying redox behaviors of pseudocapacitors. In this work, in addition to the structure directing function, RuO_2 NPs acted as a redox active material to enhance the device performance. The specific capacitances of three SCs were

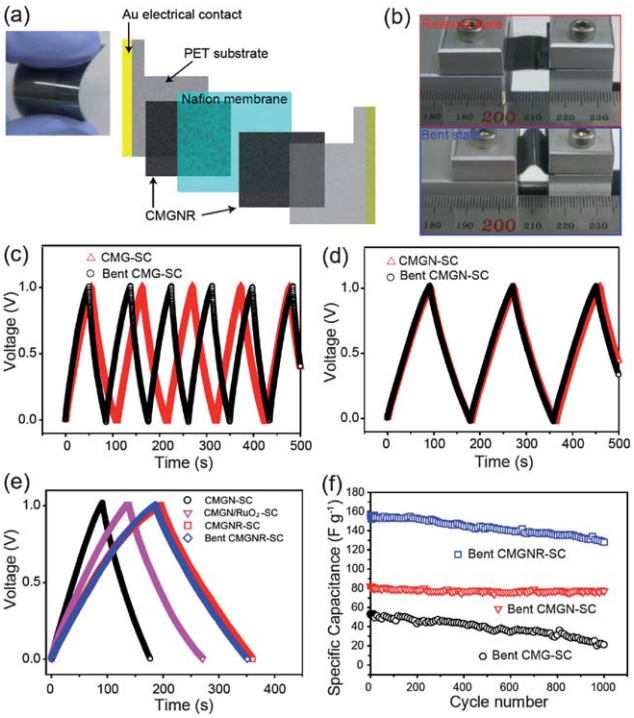

Fig. 4 (a) Photograph of a flexible CMGNR-SC and a schematic diagram of a full stacked SC device. (b) Photographs of a SC for the set-up of the bending experiments (the top image displays the relaxed state of the CMGNR-SC and the bottom image shows the bent state of the CMGNR-SC with a bending radius of 2.2 mm, corresponding to −28.5 wt% of the applied tensile strain.). (c and d) Galvanostatic charge–discharge cycles of a CMG-SC and CMGN-SC at the bent and relaxed states at a constant current of 1 A g^{-1}. (e) Galvanostatic charge–discharge curves for a CMGN-SC, CMGN/RuO_2-SC, CMGNR-SC, and bent CMGNR-SC. (f) Durability test of bending devices with a CMG-SC, CMGN-SC, and CMGNR-SC with galvanostatic charge–discharge at a constant current of 1 A g^{-1}.

measured by cycles of bending and relaxing (a bending radius: 2.2 mm and the maximum tensile strain: −28.5% described in Fig. 4b) to show the potential of CMGNR-SCs as flexible SC devices. There were no significant changes in the performance of CMGN-SCs and CMGNR-SCs at the bending states. Notably, CMGNR-SCs showed a high performance of 156 F g^{-1} even at the bending state which is in accordance with CV curves, while the specific capacitance of CMG-SCs decreased from 56.4 F g^{-1} to 27.5 F g^{-1} under identical experimental conditions (Fig. 4c). In order to confirm the durability of the CMGNR-SCs, galvanostatic charge–discharge tests at a constant current density of 1 A g^{-1} up to 1000 cycles were carried out at the bending state. Remarkably, the capacitance loss of CMGNR-SCs was calculated to be 18% after 1000 cycles at the bending state, whereas CMG-SCs revealed dramatic capacitance fading. Even during severe bending and long-term cycling tests, the CV curves of the CMGNR-SCs remained stable under the bending stress, while those of the CMG-SCs did not. The microspherical frameworks provided large surface area and facile ion transport of electrodes, while the interconnected nanosheets offered continuous electron pathways of the conductive CMGN for electroactive RuO_2 and efficient stress release. Notably, these synergistic effects of the hierarchical structure and hybrid composition enhanced the performance of energy storage devices.

The importance of the hierarchical porous structures of CMGNR microspheres was further assessed by comparing with the device performance of CMGN/RuO_2 hybrids. Note that CMGN/RuO_2 hybrids were obtained from the physical mixing of CMGNs and RuO_2 NPs, not by the self-assembly, showing the identical crystalline structure and chemical composition of RuO_2 NPs to CMGNR microspheres. Furthermore, CMGN/RuO_2 hybrids exhibited lower textural properties of 179.56 $m^2\ g^{-1}$ and 0.11 $cm^3\ g^{-1}$ compared to those of CMGNR hybrids due to the filling of RuO_2 NPs into pores (ESI, Table S1†). In particular, the capacitance of CMGN/RuO_2-SCs was measured to be 110 F g^{-1} less than 160 F g^{-1} of CMGNR-SCs, which highlights the effect of the structure on the enhancement of performance. In addition, the highest value of CMGNR-SCs shows a two-fold increase over that of RuO_2/ionic liquid/CMG film based symmetric SCs, and is even similar to the RuO_2/ionic liquid/CMG film based asymmetric SCs.[21] This result was attributed to the large surface area of hierarchical spheres of CMGNR sheets. The performance durability and flexibility of CMNGR-SCs were much better than those of CMGN/RuO_2-SCs observed from 1000 charge–discharge cycles at the bending state. CMGN/RuO_2-SCs revealed a capacitance loss of 24% even at the relaxed state (ESI, Fig. S6†) and the flexibility test could not be performed due to the destruction of film consolidation. The low performance durability of CMGN/RuO_2-SCs was largely attributed to the inefficient load transfer by means of the local concentration of RuO_2 confined in the pores of CMGN hybrids. Therefore, highly porous, microspherical structures and hybrid composition of CMGNR prepared through pseudocapacitive NP-directed assembly offers the advanced electrodes for fully bendable pseudocapacitor devices.

The electrochemical impedance spectroscopy (EIS) measurement was further investigated to analyze the electrochemical properties of CMGNR-SCs (ESI, Fig. S7†). The Nyquist plots in the frequency range from 100 kHz to 0.01 Hz clearly show the semicircle-type at the end of the Warburg-type line. The charge transfer resistances were evaluated by the diameters of the semicircles using an equivalent circuit model to be 37.2 Ω for CMGN/RuO_2-SC and 14.5 Ω for CMGNR-SC. The enhanced charge transfer must be associated with both the increased contact area between the electrolyte and electrode and the efficient electrical connection between the RuO_2 and CMGN sheets in the hierarchical structure. In addition, the CMGNR-SC shows a more vertical line than the CMGN/RuO_2-SC at the low frequency region, indicating lower ion diffusion resistance in the pore structure of the CMGNR-SC compared to the CMGN-SC. Consequently, the hierarchical structure of the CMGNR-SC with its large surface area allowed an efficient and increased contact area between the active sites and electrolytes, which led to rapid ion diffusion and efficient charge transfer.

Conclusions

We demonstrated the integrative assembly of CMG nanosheets used as 2D building blocks into hierarchical microspheres with the controlled compositions. The hierarchical morphology of the CMGNR films, directed by RuO_2 NPs, was composed of the aggregates of nanosheets and NPs assembled in microspheres through the favorable interactions between CMGN nanosheets and RuO_2 NPs. From the structural aspect, the hierarchical structures provided large surface area and facile ion accessibility to storage sites, while the interconnected nanosheets offered the continuous electron pathways and mechanical integrity. The synergistic effect of CMGNR microspheres on the capacitor performance was derived from the hybrid composition consisting of pseudocapacitive RuO_2 NPs with the conductive CMGNs as well as from structural features. Consequently, the CMGNR-SCs showed that a specific capacitance as high as 160 F g^{-1} can be reached, approximately three-fold higher than that for conventional graphene SCs, and retain >95% of the maximum value even after severe bending and 1000 charge–discharge cycling tests.

Acknowledgements

We would like to thank Dr Yi Cui at Stanford University for scientific discussions. We acknowledge the financial support by both the National Research Foundation (NRF) funded by the Korean Government (MEST) (20090063004) and NRF-2010-C1AAA001-0029018 and Basic Science Research Program through the National Research Foundation of Korea (NRF) funded by the Ministry of Education, Science and Technology (2011-0007677).

Notes and references

1 R. Liu, J. Duay and S. B. Lee, *Chem. Commun.*, 2011, **47**, 1384.
2 P. Simon and Y. Gogotsi, *Nat. Mater.*, 2008, **7**, 845.
3 C. Liu, F. Li, L.-P. Ma and H.-M. Cheng, *Adv. Mater.*, 2010, **22**, E28.
4 Y. Sun, X. Hu, W. Luo and Y. Huang, *ACS Nano*, 2011, **5**, 7100.
5 P. J. Hall, M. Mirzaeian, S. I. Fletcher, F. B. Sillars, A. J. R. Rennie, G. O. Shitta-Bey, G. Wilson, A. Cruden and R. Carter, *Energy Environ. Sci.*, 2010, **3**, 1238.
6 K. Chang and W. Chen, *ACS Nano*, 2011, **5**, 4720.
7 J. Wang, K. K. Manga, Q. Bao and K. P. Loh, *J. Am. Chem. Soc.*, 2011, **133**, 8888.
8 R. Liu, J. Duay and S. B. Lee, *ACS Nano*, 2011, **5**, 5608.
9 Y. Sun, Q. Wu and G. Shi, *Energy Environ. Sci.*, 2011, **4**, 1113.
10 S. Chen, J. Zhu, X. Wu, Q. Han and X. Wang, *ACS Nano*, 2010, **4**, 2822.
11 L. Yang, S. Cheng, Y. Ding, X. Zhu, Z. L. Wang and M. Liu, *Nano Lett.*, 2012, **12**, 321.
12 J. R. Miller and A. F. Burke, *Electrochem. Soc. Interface*, 2008, **17**, 53.
13 N. Armaroli and V. Balzani, *Energy Environ. Sci.*, 2011, **4**, 3193.
14 X. Zaho, B. M. Sánchez, P. J. Dobson and P. S. Grant, *Nanoscale*, 2011, **3**, 839.
15 Q. Wu, Y. Xu, Z. Yao, A. Liu and G. Shi, *ACS Nano*, 2010, **4**, 1963.
16 F. Meng and Y. Ding, *Adv. Mater.*, 2011, **23**, 4098.
17 B. G. Choi, J. Hong, W. H. Hong, P. T. Hammond and H. S. Park, *ACS Nano*, 2011, **5**, 7205.

18 C. Meng, C. Liu, L. Chen, C. Hu and S. Fan, *Nano Lett.*, 2010, **10**, 4025.
19 Y. Li, K. Sheng, W. Yuan and G. Shi, *Chem. Commun.*, 2013, **49**, 291.
20 Y.-R. Kang, Y.-L. Li, F. Hou, Y.-Y. Wen and D. Su, *Nanoscale*, 2012, **4**, 3248.
21 B. G. Choi, S.-J. Chang, H.-W. Kang, C. P. Park, H. J. Kim, W. H. Hong, S. Lee and Y. S. Huh, *Nanoscale*, 2012, **4**, 4983.
22 C. Li and G. Shi, *Nanoscale*, 2012, **4**, 5549.
23 Z.-S. Wu, D.-W. Wang, W. Ren, J. Zhao, G. Zhou, F. Li and H.-M. Cheng, *Adv. Funct. Mater.*, 2010, **20**, 3595.
24 B. G. Choi and H. S. Park, *ChemSusChem*, 2012, **5**, 709.
25 J. Zhang, J. Jiang, H. Li and X. S. Zhao, *Energy Environ. Sci.*, 2011, **4**, 4009.
26 B. G. Choi and H. S. Park, *J. Phys. Chem. C*, 2012, **116**, 3207.
27 B. G. Choi, H. S. Park, T. J. Park, M. H. Ynag, J. S. Kim, S.-Y. Jang, N. S. Heo, S. Y. Lee, J. Kong and W. H. Hong, *ACS Nano*, 2010, **4**, 2910.
28 W. S. Hummers and R. E. Offeman, *J. Am. Chem. Soc.*, 1958, **80**, 1339.
29 H.-S. Nam, K.-S. Jang, J. M. Ko, Y.-M. Kong and J.-D. Kim, *Electrochim. Acta*, 2011, **56**, 6459.